Langmuir

Article

pubs.acs.org/Langmuir

pH-Dependent Aggregation and Disaggregation of Native β-Lactoglobulin in Low Salt

Yunfeng Yan,[†,‡] Daniel Seeman,*[,†] Bingqian Zheng,[†] Ebru Kizilay,[†] Yisheng Xu,[†,§] and Paul L. Dubin*[,†]

[†]Department of Chemistry, University of Massachusetts—Amherst, Amherst, Massachusetts 01003, United States

[‡]Department of Chemistry, Shanghai Normal University, Shanghai 200234, China

[§]Department of Materials Science and Engineering, Cornell University, Ithaca, New York 14853, United States

Supporting Information

ABSTRACT: The aggregation of β-lactoglobulin (BLG) near its isoelectric point was studied as a function of ionic strength and pH. We compared the behavior of native BLG with those of its two isoforms, BLG-A and BLG-B, and with that of a protein with a very similar pI, bovine serum albumin (BSA). Rates of aggregation were obtained through a highly precise and convenient pH/turbidimetric titration that measures transmittance to ±0.05 %T. A comparison of BLG and BSA suggests that the difference between pH_{max} (the pH of the maximum aggregation rate) and pI is systematically related to the nature of protein charge asymmetry, as further supported by the effect of localized charge density on the dramatically different aggregation rates of the two BLG isoforms. Kinetic measurements including very short time periods show well-differentiated first and second steps. BLG was analyzed by light scattering under conditions corresponding to maxima in the first and second steps. Dynamic light scattering (DLS) was used to monitor the kinetics, and static light scattering (SLS) was used to evaluate the aggregate structure fractal dimensions at different quench points. The rate of the first step is relatively symmetrical around pH_{max} and is attributed to the local charges within the negative domain of the free protein. In contrast, the remarkably linear pH dependence of the second step is related to the uniform reduction in global protein charge with increasing pH below pI, accompanied by an attractive force due to surface charge fluctuations.

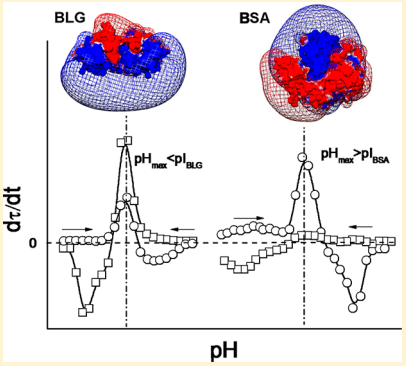

INTRODUCTION

The aggregation of proteins in their native state, an effect predominant at low ionic strength and pH near pI, is a reflection of their surface properties, in particular, the distribution of charged domains. In contrast to unfolding aggregation, native state aggregation involves interactions among hydrated protein surfaces. Without the exposure of solvophobic groups, the aggregation rate no longer depends on the kinetics of an array of transient intermediates and exhibits a higher degree of reversibility. To the extent that the limited states involved in the aggregation process are well defined, the aggregation kinetics can be analyzed from the perspective of energetics. Surface charges and their distributions then become the focus of interprotein and interparticle interactions. The diminished role of primary structure means that the aggregation of folded proteins is less protein-specific, and predictive rules based on protein tertiary structure and charge anisotropy are possible.

The association of folded proteins is of considerable importance for pharmaceutical formulation stability[1−3] and is likely to influence subsequent behavior under more extreme conditions. However, current concerns about protein conformational diseases[4] have led to a focus on the irreversible association of unfolded precursors. Unfolding aggregation requires the disruption of secondary or tertiary structure and therefore the disturbance of the numerous hydrophobic and hydrogen-bonding interactions that stabilize the native state. Proteins with various primary structures show different aggregation mechanisms, manifested in a variety of intermediates, aggregate structures, and critical temperatures. Because different regions of the protein surface become exposed and engaged in short-range interactions, unfolding aggregation can be irreversible and the mechanisms can also be highly protein-specific.[5] The corresponding numerous forms of denaturing aggregation have led to several attempts at aggregation classification − with some referring to the mechanism and some referring to the size, morphology, and reversibility of aggregates.[4] However, no general rules can be proposed to relate the sequence arrangement to the unfolding aggregation behavior, which is often observed to occur irreversibly, particularly under extreme conditions.

The characteristic reversibility of aggregation in the native state arises from the absence of high-energy unfolded intermediates subject to a new set of short-range interactions.[6] For intrinsically reversible native state aggregation,[7] the interactions involved can be better understood as involving only the hydrated protein surface.[8] Interprotein interactions may be resolved into enthalpic and entropic contributions,[9] in a

Received: July 28, 2012
Revised: February 28, 2013
Published: March 5, 2013

   dx.doi.org/10.1021/la400258r | Langmuir 2013, 29, 4584−4593

way almost impossible when subject to ongoing protein conformational changes.[9] The fact that native state aggregation, isoelectric precipitation, is suppressed by salt reveals the electrostatic origin of these contributions and suggests considerations of protein charge anisotropy.[10,11] Protein charge anisotropy is characterized by an asymmetric distribution of charge domains on a protein such that there are similar magnitude repulsive and attractive interactions present between like-charged proteins near the pI. Such charge patches are necessary to explain instances of attractive interactions between proteins and polyelectrolytes observed on the "wrong side" of the isoelectric point for which neither net charge nor highly short-range interactions would provide an adequate explanation.[12]

Electrostatic interactions among native proteins govern both the aggregation process and the structure of the final aggregate. When self-association involves electrostatic interactions, their long-range nature means that spatial separation, the first step of disaggregation, can be accomplished through changes in pH and ionic strength without exposure of hydrophobic residues. Resolvation, screening by small ions, or repulsive forces arising from changes in pH then compensates for the loss of interprotein attractive forces. Those pairwise interactions can be defined at specified conditions of pH, ionic strength, and temperature.[13] Resolution into enthalpic and entropic contributions[14] is possible when the initial and final states are well-defined and kinetics do not dominate. Modeling can then help to predict the geometry of multimers and to resolve equilibrium association constants for cognate protein−protein interactions into k_{on} and k_{off}.[15,16] Because protein−protein interactions involve solvent-accessible surfaces, protein charge anisotropy is often a contributing factor.[17,18]

The role of charge anisotropy in native state aggregation is revealed by the tendency of proteins to become insoluble at pH near the isoelectric point.[19] Because the net charge is near zero, electrostatic attractions can come only from charge asymmetry that can be visualized by computational methods based on protein structure (from the RCSB Protein Data Bank) and protein charge curves.[12] However, the correlation of protein charge with aggregation kinetics must take into account the mechanism of aggregation and deal with simultaneous equilibrium and kinetic behavior where subsequent steps governed by transient intermediates may be rate-determining.[20] Clustering or later-stage monomer consumption can be influenced by the structure of aggregates, the assembly of which is conveniently described by fractal dimensions.[21] In addition, later stages of aggregation prior to irreversible association can be subject to hysteresis because competing disaggregation may proceed by a different pathway.[22,23] Nevertheless, strong evidence of correlations between the protein surface charge state and native state aggregation rates prior to loss of solubility has been gleaned from turbidimetric measurements.[24−26] β-Lactoglobulin (BLG) with two isoforms that differ with respect to a charge patch should provide an example of such behavior.[24]

The aggregation of β-lactoglobulin (BLG) has probably been studied more than that of any other protein. The great majority of these studies have involved denaturing conditions[27,28] (e.g., extremes in pH or temperature because of their relevance to food and dairy processing[29,30]). The heat-induced aggregation of BLG is sometimes used as a general model for fibril formation,[31,32] a process that is implicated in neurodegenerative diseases.[33] Although many papers on denaturing aggregation focus on kinetics,[34,35] studies of the native state aggregation of BLG mainly deal with the equilibrium association of multimers or oligomers. Major findings include (1) the formation of dimers in equilibrium with monomers at $3 < pH < 9$[36−39] enhanced by increasing ionic strength I[38,40−42] and (2) the formation of higher-order multimers at pH 4 to 5, which for the case of an octamer[42−45] shows an opposite ionic strength dependence, shifting toward the dimer with added salt, but other reports suggest that the tetramer and hexamer could coexist.[46] Such equilibrium behavior seems to be typical for BLG at $I \geq 0.1$ M at pH far from its pI, where open-ended aggregation is avoided, although the distinction between multimerization and aggregation becomes less clear when the products of the association are small (e.g. clusters containing relatively small numbers of proteins[47]).

Kinetically controlled aggregation of BLG in the native state is typical at $I < 0.01$ M, especially at pH near pI.[24,46,48] Kumosins et al.[46] concluded from sedimentation kinetics that the aggregation of BLG is the sum of three possible interactions, namely, A−A and B−B self-interactions and A−B interactions. Timasheff and Townend[48] expanded on this, concluding that the aggregation of BLG is due primarily to a single isoform, namely, BLG-A. Majhi et al.[24] found two processes: an initial fast consumption of the BLG dimer to form an aggregate of intermediate size, followed by slow growth of the aggregates. The maximum aggregation rate occurred near pH 4.6, below the pI of 5.2, and the pH dependence of the initial aggregation rate was highly asymmetric. At pH 5.0, the initial rate increased with $1/I$. This open-ended aggregation at pH ≠ pI was attributed to the charge anisotropy of native BLG that was visualized by computer modeling. Such visualization was used to explain the dramatic effect on the aggregation rate when residues in BLG-B (gly64, ala118) are replaced in BLG-A (asp64, val118). However, the nature of the proposed two-step mechanism was not clearly elucidated, and little attention was paid to the role of pH-dependent disaggregation.

Here we consider the mechanism of pH-induced BLG native state aggregation in the vicinity of pI, with particular attention to two factors not previously examined: (1) the strong effect of the direction of pH adjustment on both aggregation and disaggregation kinetics, and (2) the nature of the two characteristic rate processes and their relationships to net versus local protein charge.[42,43] We used turbidimetric pH titrations (type 1 titration) as a convenient and effective method for measuring aggregation rates as a function of pH and the time dependence of turbidity to resolve and quantitate pH effects on the two rates. Dynamic light scattering (DLS) was used to evaluate the kinetics in terms of hydrodynamic diameters and scattering intensity under conditions where the two steps are easily resolved as revealed from titration experiments. Static light scattering (SLS) was employed to evaluate the fractal structure of quenched aggregates at two pH values corresponding to maximum values of the two rates. Electrostatic protein modeling was employed to support two distinct molecular descriptions for these processes. Finally, we show the broad and general significance of these approaches with reference to BSA as an example of protein with charge anisotropy distinct from that of BLG.

EXPERIMENTAL SECTION

Materials. Native bovine β-lactoglobulin (BLG, 18 kDa, pI = 5.2) was a gift from C. Schmitt (Nestlé, Lausanne; >97%, batch number JE 001-8-415, 55.4% BLG-A and 41.6% BLG-B). Isoforms of BLG (BLG-

dx.doi.org/10.1021/la400258r | Langmuir 2013, 29, 4584−4593

A and BLG-B) were from Sigma-Aldrich (lot nos. 097K7010 and 048K7003 V, respectively). Fatty acid-free bovine serum albumin fraction V (BSA, 68 kDa, pI = 4.9, >99%) was Calbiochem lot D00096763. NaCl and standard NaOH and HCl solutions were purchased from Fisher Scientific. Milli-Q water was used in all sample preparation.

Turbidimetry. Turbidimetric titrations were performed by the addition of either 0.1 N NaOH (forward titration) or 0.1 N HCl (backward titration) to a 15 mL protein solution with stirring and the simultaneous monitoring of pH and transmittance at 25 °C. It is conventional to report τ as 100 − %T, a unitless quantity that is linear with turbidity over a certain range of transmittance. It is convenient to describe it in this form because it absorbs terms such as the extinction coefficient, which would otherwise be poorly defined for such systems. The rate of pH change was kept at 0.2 pH unit/min in all titrations except for the experiments in Figure S1. For kinetics experiments, protein solutions were prepared at pH 9 and brought to the desired pH by the addition of 0.1 N HCl in 15 s. The transmittance of protein solutions was measured using a Brinkmann PC 800 colorimeter equipped with a 420 nm filter and a 1 cm path length fiber optic probe, calibrated to 100% transmittance with Milli-Q water. Instrument drift during a single measurement was less than 0.05 %T after a 30 min warm-up. pH was measured with a Corning 240 pH meter. Samples were filtered with a 0.22 μm membrane (Millipore) before titration. With this technique, turbidity measurements are precise to ±2 ppt and highly robust, with repeatability demonstrated by the precise reproduction of the I^{-1} dependence of BLG aggregation previously measured[24] (Figure S3).

Dynamic Light Scattering (DLS). DLS was carried out at 25.0 °C with a Malvern Zetasizer Nano ZS instrument equipped for backscattering at 173° with a 633 nm He−Ne laser. Protein solutions were adjusted rapidly from a nonaggregating pH (7.0) to pH 4.9 or 5.1. DLS measurements were started within 30 s of the pH adjustment. The distributions of the mean apparent translational diffusion coefficients (D_T) were determined by fitting the DLS autocorrelation functions using non-negative constrained least-squares (NNLS). The robustness of this algorithm vis-à-vis CONTIN has been amply demonstrated, even for systems with more than two decay modes. The distribution of the apparent hydrodynamic radii (R_{app}) was obtained from the distribution of mean apparent translational diffusion coefficients (D_T) via

$$R_{app} = \frac{kT}{6\pi\eta D_T} \quad (1)$$

where k is the Boltzmann constant, T is the absolute temperature, and η is the solvent viscosity, which was assumed to be that of water.

Static Light Scattering (SLS). SLS experiments were performed using a BI-200 SM goniometer and BIC-2030D photon counting system (Brookhaven Instruments Inc.) with an Omnichrome Ar ion laser (100 mW, λ = 488 nm) at ambient temperature, ∼25 °C. The scattering intensity was measured as a function of scattering angle between 75 and 120°. Fractal dimensions (D_f) were extracted from angle dependence in the high-q limit via linearization[49] of the scattering data using the relation

$$I(q) \propto q^{-D_f} \quad (2)$$

where $I(q)$ is the scattering intensity and the scattering vector q is $(4\pi n/\lambda)\sin(\theta/2)$, with n the refractive index of the fluid, λ the wavelength, and θ the scattering angle. BLG aggregation in 0.01 M NaCl was initiated by pH adjustment from 7.0 to either 4.9 or 5.1 and sustained for 5−20 min. Aggregation was quenched by rapid adjustment from the aggregating pH to pH 4.4, at which point the aggregate size was found by DLS to no longer change with time. Each SLS measurement was made in replicate over the course of 2 h to ensure that quenched samples were invariant with respect to time.

Computational Methods. DelPhi V. 4r1.1 was used to model the electrostatic potential around the protein as a function of pH and ionic strength. pdb 3V03 (BSA monomer) and 1BEB (BLG dimer) were taken from the RCSB Protein Data Bank (http://www.rcsb.org). The amino acid charges were generated using the spherical-smeared-charge model proposed by Tanford on the basis of titration curves of BLG and BSA.[50]

RESULTS

Turbidimetric pH Titrations. The increase in turbidity upon addition of acid or base, as shown for the curve of larger magnitude in Figure 1a, summarizes the accumulation of soluble aggregates and their subsequent redissolution with diminishing pH. Even at fixed protein concentration and ionic strength, the turbidity, as a kinetic variable, is sensitive to the elapsed time between titrant increments, which is presumably responsible for deviations in absolute turbidity among duplicate runs; this did not exceed 15% (relative). However, the pH corresponding to the maximum change in turbidity $(d\tau/dt)_{max}$ did not vary. The rate of titrant addition was controlled to ensure that dpH/dt is constant; consequently, the instantaneous rate of aggregation at any pH ($(d\tau/dt)_{pH}$) is given by $(d\tau/dpH)(dpH/dt)$. Hence, the plot in Figure 1b essentially describes the pH dependence of the instantaneous rate of aggregation. As will be shown below, $(d\tau/dt)_{pH}$ obtained in this way is remarkably similar to $(d\tau/dt)_{t=0}$ at fixed pH so that the inflection points indicated by the vertical dashed lines are the pH's of the maximum aggregation rate. It is of interest to note the crossing point of the two curves in Figure 1a, which correspond closely to the identical pH positions of the maxima in Figure 1b. The absence of any effect of the titration direction on the rate suggests that the process is controlled by free protein and not prior aggregates. Furthermore, the pH values at the turbidity maxima can be directly confirmed as conditions of constant turbidity (Figure S2 in the Supporting Information). The magnitude of accumulated aggregate τ_{max} clearly depends on the direction of titration (Figure 1a). This may indicate differences in aggregate structure, which also would lead to differences in disaggregation. However, regardless of the titration *direction*, the curves cross at the inflection point (see

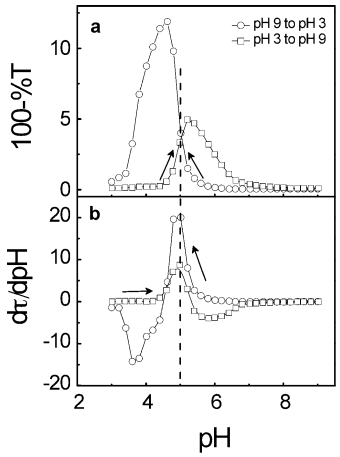

Figure 1. (a) Type 1 titrations of 1.0 g/L BLG in 0.0045 M NaCl. (b) dτ/dpH vs pH. The rate of addition of HCl or NaOH was 0.2 pH unit/min. The titration directions indicated by arrows are (□) low to high pH and (○) high to low pH. The vertical dashed line corresponds to the inflection points (maximum aggregation rates) for both directions. −dτ/dpH is shown for pH 9 → 3 to adjust for the trivially negative values of dpH: negative values in (b) correspond to disaggregation.

dx.doi.org/10.1021/la400258r | Langmuir 2013, 29, 4584−4593

also $d\tau/dpH$ in Figure 1b): the maximum aggregation rate occurs at the same pH.

To demonstrate the utility of turbidimetric pH titrations, we carried out titrations with acid at ionic strengths I ranging from 0.0045 to 0.1 M (NaCl). The ionic strength dependence of the inflection points $(d\tau/dpH)_{max}$ showed nearly the same I^{-1} dependence (Figure S3) as seen previously for the initial rate at fixed pH $(d\tau/dt)_0$.[24] As expected, the maximum turbidity depended on the rate of titration, increasing ca. 40% with a 3-fold decrease in (dpH/dt), but the characteristic pH's of τ_{max} and $(d\tau/dt)_{max}$ (Figure S1) were independent of (dpH/dt). The pH titrations thus yield, more conveniently, very similar results to the more laborious time-dependent studies at fixed pH.

Identification of Two Steps. The extent of aggregation of BLG increases with pH from 4.4 to 4.8 and decreases as the pH increases from 5.1 to 5.7 (Figure 2), but the pH dependence of

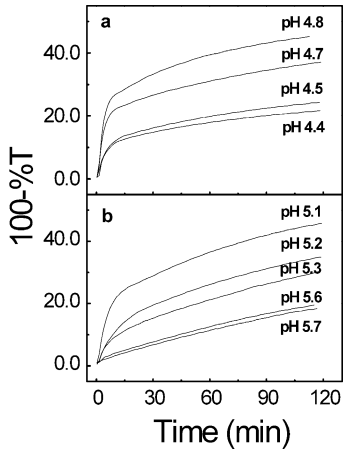

Figure 2. Turbidity vs time for 1.0 g/L BLG (1.3:1 A/B), I = 0.0045 M. (a) pH 4.4−4.8 and (b) pH 5.1−5.7.

the amount of aggregate is seen to be mainly determined in the first ca. 10 min. In other words, a fast initial step is followed by a slow second step. The pH dependences of the aggregation rates for the fast initial step (t < 10 min) and the following slow step (45 < t < 90 min) are reported as $(d\tau/dt)_0$ and $(d\tau/dt)_2$ in Figure 3a and b, respectively. The pH dependence of $(d\tau/dt)_0$ is symmetric around a maximum at pH 4.9 (i.e., below pI = 5.2). In contrast, $(d\tau/dt)_2$, typically ca. 25 times smaller than $(d\tau/dt)_0$, is remarkably linear with pH, attaining a maximum at pI. In addition, the two steps show different ionic strength dependences (i.e., the aggregation rate is linear with I^{-1} for the initial step and with $I^{-0.25}$ for the second step (Figure 4)). The implications regarding the different mechanisms and the respective roles of protein charge anisotropy in the two steps will be discussed below.

Structure of BLG Aggregates. Dynamic light scattering was used to study the aggregation of 1.0 g/L BLG at pH 4.9 and 5.1, conditions that correspond to the apparent aggregation rate maxima in the initial and second steps, respectively. At pH 4.9, where the initial rate dominates, hydrodynamic diameters (Figure 5a) grow to over a micrometer in t < 10 min, during which time the scattering intensity increases dramatically (Figure 5c). In contrast, at pH 5.1, a gradual increase in size is observed (Figure 5b) along with an almost negligible increase in scattering intensity (Figure 5d). The increase in diameters seen at pH 4.9 at short time together with the relatively smaller

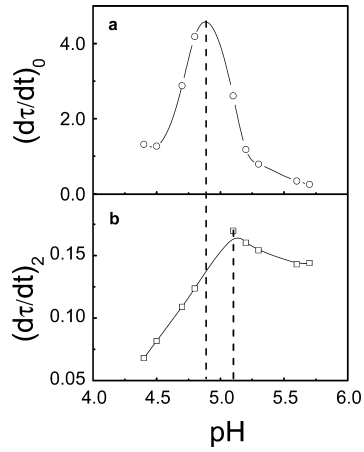

Figure 3. Aggregation rate $(d\tau/dt)$ vs pH from Figure 2. (a) Initial rate $(d\tau/dt)_0$ and (b) aggregation rate for the second step $(d\tau/dt)_2$. The vertical dashed lines denote the pH's for the maxima of $(d\tau/dt)_0$ and $(d\tau/dt)_2$. Note the different scales for plots a and b showing the dominant effect of the initial rate.

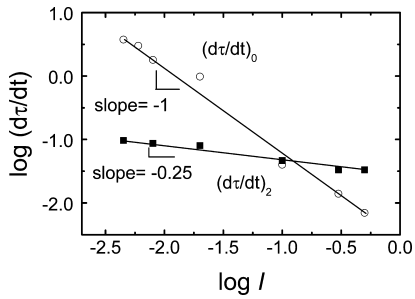

Figure 4. Logarithmic plot of $d\tau/dt$ and I (open symbols for the initial rate, filled symbols for the second step) at pH 5.0. The slopes are −1 and −0.25 for $(d\tau/dt)_0$ and $(d\tau/dt)_2$, respectively. Data are reproduced from a previous paper.[24]

effect at pH 5.1 suggests that the initial rate is controlled by the formation of nuclei, and the second step involves the growth of preformed nuclei. Notably absent is any evidence of species of intermediate size, indicating that aggregates are formed from BLG dimers (possibly in equilibrium with monomers) with no involvement of multimers such as tetramers and hexamers.

The apparent quenching of aggregate growth (Figures 1b and S2) arises from a balance of aggregation and disaggregation rates at a particular pH (i.e., 4.4). Adjustment from aggregating conditions (pH 4.9 or 5.1) to this quenching condition halts the growth of protein aggregates. SLS results under these two conditions are shown in Figures 6. Fractal dimensions, a power law describing the distribution of mass or scattering centers within an aggregate, were measured for each quenched sample.

SLS results for the sample quenched from pH 4.9 (Figure 6a) where step one is maximal show that the apparent D_f of BLG aggregates increases continuously before finally converging to a limiting value of 3.0, which is consistent with a fully compact structure. At pH 5.1 (Figure 6b), the increase in fractal dimension is comparable but a lower limiting value is reached, indicating that these aggregates remain somewhat fractal in nature even at t = 20 min (Figure 6c). The D_f increases slowly during the first ∼10 min, a lag time displayed at both pH's. In this first step the structures formed are loose, allowing for the rapid packing of free BLG into the aggregate. The values of D_f would seem to preclude both classical diffusion- and reaction-

dx.doi.org/10.1021/la400258r | Langmuir 2013, 29, 4584−4593

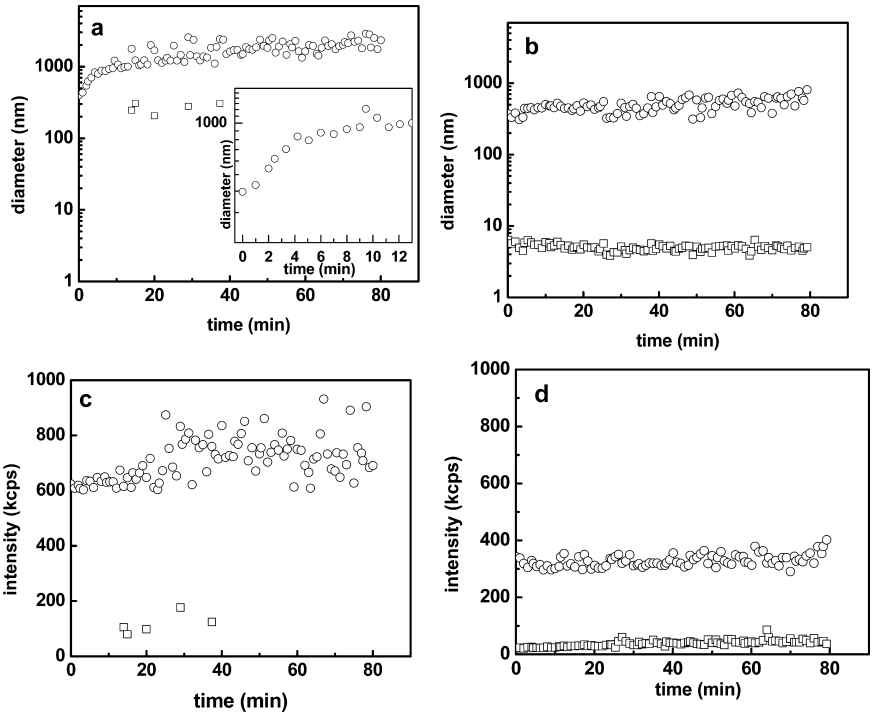

Figure 5. DLS kinetics of 1.0 g/L BLG in I = 0.01 M at (a, c) pH 4.9 and (b, d) pH 5.1. (○) Slow mode and (□) fast mode obtained from the intensity-weighted distribution of apparent diameters. The inset in plot a is an expansion of the first 13 min.

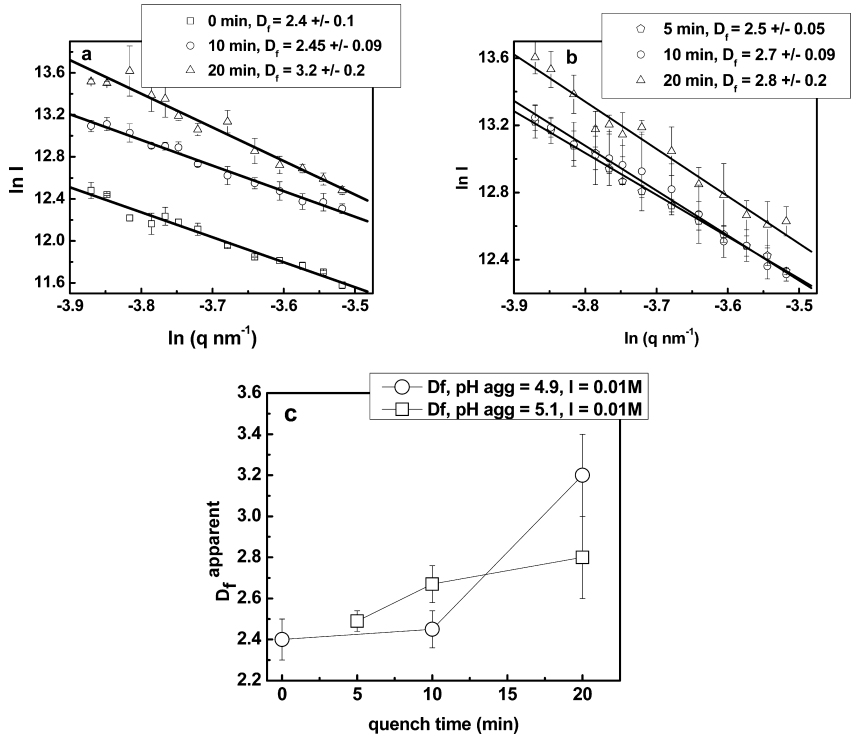

Figure 6. SLS of 1 g/L BLG in I = 0.01 M quenched by adjustment to pH 4.4 after a fixed amount of time. BLG aggregation is induced at (a) pH 4.9 and (b) pH 5.1. (c) Apparent D_f as a function of quench time.

limited cluster−cluster aggregation[51] but are consistent with an initial nucleation step represented by diffusion-limited particle−cluster aggregation.[51] By the final quench point, aggregates are no longer fractal in nature, possibly explained by a switch to reaction-limited particle cluster aggregation[51] in which the close packing of free protein results in a nearly homogeneous structure. At pH 5.1, such nucleation occurs more slowly, leading to a smaller observed fractal dimension at the final quench point.

In the absence of intermediate species (e.g., oligomers), the increase in turbidity must be attributed to the formation of aggregates that grow in size and decrease in number. With

dx.doi.org/10.1021/la400258r | Langmuir 2013, 29, 4584−4593

appropriate assumptions about their density, based on fractal dimensions, it is possible to estimate that the number of dimers per aggregate increases from roughly 2×10^4 to 5×10^6 over the first 20 min, with a concomitant 250-fold decrease in the number of aggregates. The present results do not indicate whether this occurs by aggregate fusion or dimer consumption, which is the subject of an ongoing size exclusion study.

Aggregation of BLG Isoforms. The marked difference between the amplitudes of aggregation of BLG variants A and B provides strong evidence of the effect of charge anisotropy that arises from the replacement of uncharged amino acid glycine by aspartic acid in BLG-A, adding two additional negative charges per dimer, as previously noted.[52] Native BLG can be found under dimer dissociation conditions,[24] to contain roughly equal numbers of the A and B monomers, but the distribution among the three possible dimers is not always clear. Mass spectra of Sigma BLG-A prepared at pH 4.5 showed unresolved dimer peaks,[53] but more recently obtained higher-resolution spectra (Figure S4) suggest that the AA and BB dimers that predominate in native BLG may dissociate to form the AB heterodimer. This complexity provides additional motivation to examine the aggregation behavior of the homodimers.

Turbidimetric pH titrations of AA and BB are shown in Figure 7a,b. Regardless of the direction of titration, aggregation

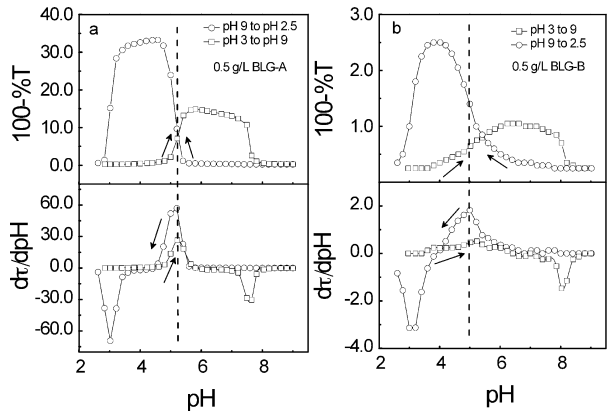

Figure 7. Type 1 titrations and dτ/dpH vs pH for (a) 0.5 g/L BLG-A and (b) 0.5 g/L BLG-B. The rate of addition of HCl or NaOH was 0.2 pH unit/min. The dashed line corresponds to the pH of the maximum aggregation rate, independent of direction. Titration direction: (□) low to high and (○) high to low. I = 0.0045 M. We show −dτ/dpH to adjust for the trivially negative values of dpH for pH 9 → 3 in the lower curves.

rates are larger by factors of 20−30 for the A dimer. For both titration directions, the aggregation of BLG-A begins only at pH within 0.5 pH unit of the pI. For titration with base, significant disaggregation commences at pH 7.5, and for titration with acid, at pH 3.5. The equivalence of crossing points with points of maximum aggregation rate noted in Figure 1 is notably absent in Figure 7b because of the large difference in rates. Further comparisons of BLG-B with BLG-A are complicated by the different magnitudes mentioned above.

Turbidimetric pH Titration of BSA. BLG aggregates most strongly at pH < pI because of its negative charge patch.[24] Because BSA, in contrast to BLG, has a positive charge patch,[12] comparative titrations were done with BSA to reinforce this relationship with protein charge anisotropy. The results of this type 1 titration for BSA in Figure 8 may be compared to the analogous plot for BLG in Figure 1. As is the case for BLG, the

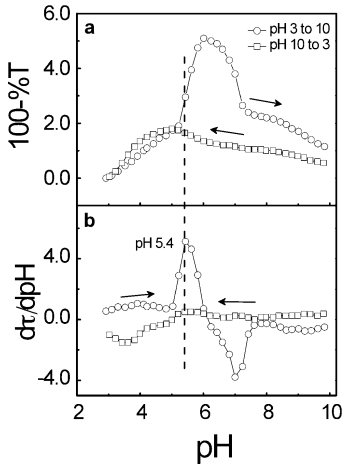

Figure 8. (a) Type 1 titrations of 1.0 g/L BSA in 0.0045 M NaCl with NaOH or HCl (arrows). (b) dτ/dpH vs pH. The rate of addition of HCl or NaOH was 0.2 pH unit/min. The titration directions indicated by arrows are (○) low to high pH and (□) high to low pH. The vertical dashed line corresponds to the inflection points (maximum aggregation rates) for both titration directions. −dτ/dpH is shown for pH 9 → 3 in plot b to adjust for the trivially negative values of dpH.

pH for the maximum aggregation rate of BSA does not depend on the titration direction, but in contrast to BLG, the pH_{max} for BSA (5.4) is well *above* its pI (4.9).

DISCUSSION

Forward and Backward pH Titrations. Turbidimetric pH titration is a convenient method for the study of electrostatically driven native protein aggregation, particularly when the titration rate (dpH/dt) is constant. The instantaneous aggregation rate $(d\tau/dt)_{pH}$ at any pH is then obtained by $(d\tau/dpH)(dpH/dt)$. For example, with dpH/dt = 0.2 pH units min^{-1}, we obtain from the acid titration in Figure 1b an aggregation rate of 4.0 min^{-1}. The kinetic measurement at pH 4.8 (Figures 2 and 3) gives the initial rate of $d\tau/dt$ = 4.1 min^{-1}. The validation of this method was also confirmed by the ionic strength dependence of the aggregation rate from turbidimetric pH titration at varying I (Figure S3), similar to previous results.[24] The inflection points in Figure 1 correspond to the pH's of the maximum aggregation rate, and the turbidity maxima correspond to pH values at which turbidimetric rates of association and dissociation are equal (Figure S2). These observations should apply generally to the pH dependence of native state protein aggregation.

First Aggregation Step. The crossing point at pH 5.0 in Figure 1 shows the importance of the direction of titration but also indicates a condition at which the rate of aggregation is independent of the sample history. The strong influence of titration direction is in contrast to the pH-induced aggregation of Zn-free insulin that appears to be essentially reversible.[54] The nearly symmetrical behavior in that case (titration curves did *not* cross) was related to the dipole-like behavior of the protein, with high- and low-pH deviations from pI essentially leading to charge mirror images. The dramatically different shapes of low-to-high and high-to-low curves indicate important effects of the surface charge distribution not reflected in |pH − pI|. However, the pH's at maximum $d\tau/dt$ (5.0) are independent of direction, because they reflect only rates of change regardless of prior accumulations of aggregate and thus depend uniquely on the state of the free protein. This point is

dx.doi.org/10.1021/la400258r | *Langmuir* 2013, 29, 4584−4593

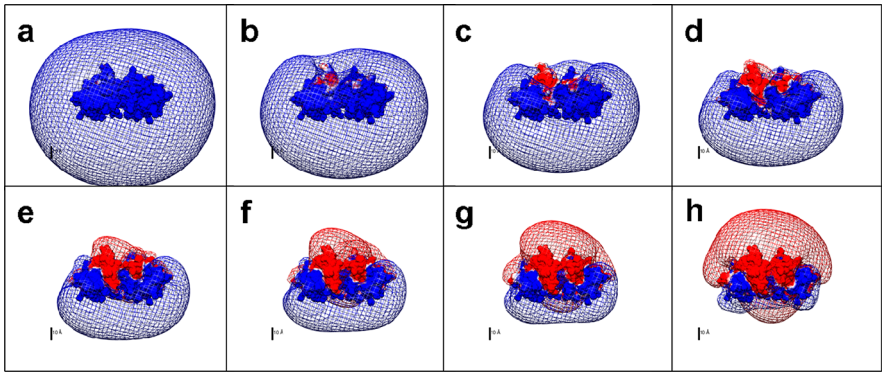

Figure 9. Electrostatic potential contours (+0.5kT/e (blue) and −0.5kT/e (red)) around the BLG dimer at ionic strength 0.0045 M. pH values and corresponding net charges: (a) 4.0, +12, (b) 4.4, +7, (c) 4.6, +6, (d) 4.8, +5, (e) 5.0, +3, (f) 5.2, 0, (g) 5.4, −2, and (h) 5.8, −3. Calculation was based on pdb id 1BEB, which has the same arrangement (and number) of charged residues as BLG B but has an additional noncharged amino acid. The scale bar is equal to 1 nm. Dimer net charge[56] rounded to the nearest whole number.

0.2 pH unit below pI; this and the marked difference in aggregation rates for BLG-A and BLG-B[24] suggest an important role for the negative patch of BLG (Figure 9) wherein reside the additional two asp residues of the A dimer. The variation of the charge in this domain accounts for the pH dependence of aggregation, which is seen in Figure 3a to arise mainly from the first step. The impact of this first step can be understood from charge anisotropy: the onset of aggregation at pH ∼4.6 for base titration in Figure 1a corresponds to a large positive domain (Figure 9c) capable of interacting with the negative domains of several others, resulting in an open aggregate with a lower fractal dimension.[55] A diffusion-limited analysis of this process[24] was shown to account for the I^{-1} dependence of the initial rate shown in Figure 4. Acid titration commencing at pH ∼5.4 shows less asymmetry, which could lead to a more dense structure possibly producing higher turbidity (Figure 1a). Although the structure of the aggregate formed may depend on the direction, the state of free protein that determines the rate of the first step does not.

Second Aggregation Step. In marked contrast to the behavior of the first step, we see for $(d\tau/dt)_2$ Figure 3b, aggregation behavior that is highly asymmetric with respect to pH, with a local maximum at pI, and (b) a remarkably linear pH dependence of $d\tau/dt$ at lower pH. This linearity is consistent with the linearity of net protein charge Z with pH in this region,[56] along with maximum aggregation at pH = pI, this suggests that global charge, not anisotropy, is dominant. As seen in Figure 4, the diminution of $(d\tau/dt)_2$ with added salt also implies an electrostatic attractive force, even at pH = pI. However, $(d\tau/dt)_0$ shows a stronger ionic strength dependence, increasing with I^{-1}. This proportionality was previously explained[24] as a consequence of an increase in the target area of the protein negative domain with the square of the Debye length κ^{-1}, which leads to the observed I^{-1} dependence because for 1:1 electrolytes $\kappa^{-1} \approx 0.3/I^{1/2}$ (where the units of κ^{-1} and I are nm and M). $(d\tau/dt)_2$, however, depends on $I^{-0.25}$. Because free protein is consumed before the second step, it is necessary to identify a weakly screened attractive force between clusters of low net charge. The theory by Miklavic[57] for inhomogeneously charged surfaces at short separation describes an attractive force that becomes dominant when charges can migrate.[58,59] With any aggregating system, diffusion will eventually induce microscopic concentration fluctuations that will bring two particles to the short separation distances at which such theory becomes very relevant. The overall attraction in this treatment increases with intercharge spacing and decreases with κ^2, the first term dominating for low salt. To this effect we add a weak Z-dependent repulsion that decreases with increasing κ (i.e., increasing I). The relative magnitudes of these two opposing effects depend on the intercharge spacing of the cluster surface, which is not known, but the observed $I^{-0.25}$ dependence of the attraction reflects their sum. The treatment of Miklavic et al. suggests that a balance between attraction and repulsion dictated by charge spacing on the surface of protein clusters could lead to the observed I dependence. In summary, protein net charge Z provides a weak repulsion, and its disappearance at pH 5.2 accounts for the maximum in $(d\tau/dt)_2$ in Figure 3b. The mobility of protein charges on the cluster surface accounts for the attractive force that drives cluster−cluster association, in contrast to the fixed charges on the nonaggregated dimer that control the first step.

BLG-A and BLG-B. The influence of protein charge anisotropy, in particular, the role of the negative domain seen most clearly in Figure 9d−f, can be assessed by a comparison of BLG-A and BLG-B. The type 1 titrations in Figure 7 reveal aggregation rates an order of magnitude higher for the A isoform. Focusing first on the crossing points where turbidity is independent of the direction of titration, it is reasonable to suggest that these represent the rate of aggregation of the dimer (first step). The crossing points of pH 5.2 and 5.4 for AA and BB, respectively, suggest that an increase in pH to 5.4 for BB results in behavior similar to that of AA at pH 5.2. Thus titration with NaOH up to pH 5.0 involves more retention of net positive protein for BLG-B (pI ∼5.2) than for BLG-A (pI ∼5.1), accounting for the accumulation of fewer aggregates and the absence of a crossing point. Comparison with Figure 1 shows that the aggregation rate at pH 5.0 (high to low titration) for native BLG is lower than that for AA by a factor of 3, even though the protein concentration is twice as large for the native form. The finding that the turbidity of native BLG (Figure 1) is much smaller than the sum of the contributions of AA and BB (Figure 7) is also in agreement with earlier observations that BB suppresses the aggregation of AA.

Turbidimetric Titration of BSA. The charge anisotropy of BSA (Figure 10) is distinctly different from that of BLG. As in the case of BLG, the absence of any influence of the titration direction on the pH of the maximum aggregation rate (pH_{max}) reflects the dominant role of the charge anisotropy of the free protein. However, pH_{max} is above pI for BSA vs. below pI for BLG. There are two possible explanations for this effect. If

dx.doi.org/10.1021/la400258r | Langmuir 2013, 29, 4584−4593

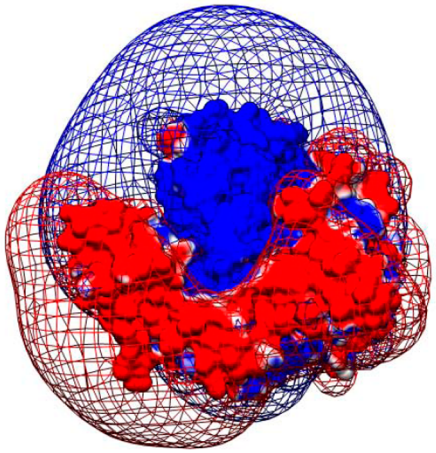

Figure 10. Electrostatic potential contours (+0.5kT/e (blue) and −0.5kT/e (red)) around BSA at an ionic strength of 0.0045 M and pH 5.4 (conditions identical to those for BLG in Figure 9g).

positive patches are stable at low pH, as is the case for BSA in the range of 4.5 < pH < 6,[60] then the aggregation rate will be determined by the expansion of the diffuse negative domain at higher pH; if a negative patch is stable at high pH, then aggregation will be enhanced by the expansion of a diffuse positive domain at lower pH. This scenario describes BSA and BLG, respectively. The second explanation involves two steps, the first some form of nucleation and the second reflecting the tendency of net charge to oppose cluster formation. Preliminary kinetics experiments suggest that this two-step mechanism is consistent even at 10-fold-higher protein concentrations. Because the two steps have different pH and concentration dependences, the transition from step 1 to step 2 during the course of a type 1 titration will depend not only on the direction of titration but also on the rate of acid/base addition and on the total protein concentration. A more detailed investigation of this scenario would involve monitoring the initial and aggregated species by DLS as a function of the direction and rate of pH change, which is beyond the scope of the current work.

CONCLUSIONS

Turbidimetric pH titrations (type 1 titration) conveniently provide accurate measurements of the pH-dependent rate of aggregation ($d\tau/dt$) of native state proteins: the pH of the maximum aggregation rate (pH_{max}) and the ionic strength dependence of ($d\tau/dt$) are equivalent to results from kinetic measurements. The results for BLG lead to the identification of two predominantly electrostatic steps. The rate of the first step, ascribed to the aggregation of free protein and dominated by charge anisotropy, is symmetrical around pH_{max} (4.9) and inversely proportional to the ionic strength. At pH_{max}, DLS kinetics shows the rapid growth of apparent size at early time relative to that at pH 5.1, whereas SLS of aggregates at both pH's shows the formation of increasingly dense structures consistent with particle−cluster aggregation. The relatively slow aggregation rate in the second step varies linearly with pH at constant I for pH < pI and is inversely proportional to $I^{0.25}$. This process is due to the association of clusters with inhomogeneous and mobile charge surfaces. The role of charge anisotropy in the first step is substantiated by the more rapid aggregation of the A isoform of BLG and by the contrasting aggregation behavior of BSA with inverted charge anisotropy.

ASSOCIATED CONTENT

Supporting Information

Type 1 titrations of BLG from high to low pH with different titration rates, times, and pH dependences of turbidity at pH 4.6. Ionic strength dependence of aggregation rates. Mass spectra of a BLG-A and BLG-B mixture. Example of the reproducibility of a type 1 titration of BLG with HCl. This material is available free of charge via the Internet at http://pubs.acs.org.

AUTHOR INFORMATION

Corresponding Author

*E-mail: dseeman@chem.umass.edu, dubin@chem.umass.edu.

Notes

The authors declare no competing financial interest.

ACKNOWLEDGMENTS

We thank Dr. Christophe Schmitt and Prof. Sven Holger Behrens for helpful discussions. B.Z. acknowledges the support of a Bradspies summer research fellowship.

REFERENCES

(1) Arosio, P.; Rima, S.; Lattuada, M.; Morbidelli, M. Population Balance Modeling of Antibodies Aggregation Kinetics. *J. Phys. Chem. B* **2012**, *116*, 7066−7075.

(2) Roberts, C. J. Kinetics of Irreversible Protein Aggregation: Analysis of Extended Lumry-Eyring Models and Implications for Predicting Protein Shelf Life. *J. Phys. Chem. B* **2003**, *107*, 1194−1207.

(3) Carpenter, J. F.; Randolph, T. W.; Jiskoot, W.; Crommelin, D. J. A.; Middaugh, C. R.; Winter, G.; Fan, Y.-X.; Kirshner, S.; Verthelyi, D.; Kozlowski, S.; Clouse, K. A.; Swann, P. G.; Rosenberg, A.; Cherney, B. Overlooking Subvisible Particles in Therapeutic Protein Products: Gaps That May Compromise Product Quality. *J. Pharm. Sci.* **2009**, *98*, 1201−1205.

(4) Frieden, C. Protein Aggregation Processes: In Search of the Mechanism. *Protein Sci.* **2007**, *16*, 2334−2344.

(5) Fink, A. L. Protein Aggregation: Folding Aggregates, Inclusion Bodies and Amyloid. *Fold. Des.* **1998**, *3*, R9−R23.

(6) Sanchez-Ruiz, J. M. Protein Kinetic Stability. *Biophys. Chem.* **2010**, *148*, 1−15.

(7) Nicolai, T.; Britten, M.; Schmitt, C. β-Lactoglobulin and WPI Aggregates: Formation, Structure and Applications. *Food Hydrocolloids* **2011**, *25*, 1945−1962.

(8) Philo, J. S.; Arakawa, T. Mechanisms of Protein Aggregation. *Curr. Pharm. Biotechnol.* **2009**, *10*, 348−351.

(9) Brady, G. P.; Sharp, K. A. Entropy in Protein Folding and in Protein-Protein Interactions. *Curr. Opin. Struct. Biol.* **1997**, *7*, 215−221.

(10) Seyrek, E.; Dubin, P. L.; Tribet, C.; Gamble, E. A. Ionic Strength Dependence of Protein-Polyelectrolyte Interactions. *Biomacromolecules* **2003**, *4*, 273−282.

(11) Park, J. M.; Muhoberac, B. B.; Dubin, P. L.; Xia, J. L. Effects of Protein Charge Heterogeneity in Protein-Polyelectrolyte Complexation. *Macromolecules* **1992**, *25*, 290−295.

(12) Grymonpre, K. R.; Staggemeier, B. A.; Dubin, P. L.; Mattison, K. W. Identification by Integrated Computer Modeling and Light Scattering Studies of an Electrostatic Serum Albumin-Hyaluronic Acid Binding Site. *Biomacromolecules* **2001**, *2*, 422−429.

(13) Dufrechou, M.; Poncet-Legrand, C.; Sauvage, F. X.; Vernhet, A. Stability of White Wine Proteins: Combined Effect of pH, Ionic Strength, and Temperature on Their Aggregation. *J. Agric. Food Chem.* **2012**, *60*, 1308−1319.

(14) Gummadi, S. N. What Is the Role of Thermodynamics on Protein Stability? *Biotechnol. Bioprocess Eng.* **2003**, *8*, 9−18.

(15) Schreiber, G.; Fersht, A. R. Rapid, Electrostatically Assisted Association of Proteins. *Nat. Struct. Biol.* **1996**, *3*, 427−431.

(16) Selzer, T.; Schreiber, G. Predicting the Rate Enhancement of Protein Complex Formation from the Electrostatic Energy of Interaction. *J. Mol. Biol.* **1999**, *287*, 409−419.
(17) Asthagiri, D.; Paliwal, A.; Abras, D.; Lenhoff, A. M.; Paulaitis, M. E. A Consistent Experimental and Modeling Approach to Light-Scattering Studies of Protein-Protein Interactions in Solution. *Biophys. J.* **2005**, *88*, 3300−3309.
(18) Liu, Y.; Fratini, E.; Baglioni, P.; Chen, W. R.; Chen, S. H. Effective Long-Range Attraction between Protein Molecules in Solutions Studied by Small Angle Neutron Scattering. *Phys. Rev. Lett.* **2005**, *95*, 118402.
(19) Mathews, C. K.; van Holde, K. E.; Ahern, K. G. *Biochemistry*, 3rd ed.; Addison Wesley Longman: San Francisco, 2000.
(20) Ferrone, F. Analysis of Protein Aggregation Kinetics. *Methods Enzymol.* **1999**, *309*, 256−274.
(21) Lin, M. Y.; Lindsay, H. M.; Weitz, D. A.; Ball, R. C.; Klein, R.; Meakin, P. Universal Reaction-Limited Colloid Aggregation. *Phys. Rev. A* **1990**, *41*, 2005−2020.
(22) Urbanc, B.; Cruz, L.; Buldyrev, S. V.; Havlin, S.; Hyman, B. T.; Stanley, H. E. Dynamic Feedback in an Aggregation-Disaggregation Model. *Phys. Rev. E* **1999**, *60*, 2120−2126.
(23) Cruz, L.; Urbanc, B.; Buldyrev, S. V.; Christie, R.; GomezIsla, T.; Havlin, S.; McNamara, M.; Stanley, H. E.; Hyman, B. T. Aggregation and Disaggregation of Senile Plaques in Alzheimer Disease. *Proc. Natl. Acad. Sci. U.S.A.* **1997**, *94*, 7612−7616.
(24) Majhi, P. R.; Ganta, R. R.; Vanam, R. P.; Seyrek, E.; Giger, K.; Dubin, P. L. Electrostatically Driven Protein Aggregation: beta-Lactoglobulin at Low Ionic Strength. *Langmuir* **2006**, *22*, 9150−9159.
(25) Xu, Y.; Seeman, D.; Yan, Y. F.; Sun, L. H.; Post, J.; Dubin, P. L. Effect of Heparin on Protein Aggregation: Inhibition versus Promotion. *Biomacromolecules* **2012**, *13*, 1642−1651.
(26) Xu, Y. S.; Yan, Y. F.; Seeman, D.; Sun, L. H.; Dubin, P. L. Multimerization and Aggregation of Native-State Insulin: Effect of Zinc. *Langmuir* **2012**, *28*, 579−586.
(27) Schmitt, C.; Moitzi, C.; Bovay, C.; Rouvet, M.; Bovetto, L.; Donato, L.; Leser, M. E.; Schurtenberger, P.; Stradner, A. Internal Structure and Colloidal Behaviour of Covalent Whey Protein Microgels Obtained by Heat Treatment. *Soft Matter* **2010**, *6*, 4876−4884.
(28) Schmitt, C.; Bovay, C.; Rouvet, M.; Shojaei-Rami, S.; Kolodziejczyk, E. Whey Protein Soluble Aggregates from Heating with NaCl: Physicochemical, Interfacial, and Foaming Properties. *Langmuir* **2007**, *23*, 4155−4166.
(29) Davis, P. J.; Williams, S. C. Protein Modification by Thermal Processing. *Allergy* **1998**, *53*, 102−105.
(30) Ehn, B. M.; Ekstrand, B.; Bengtsson, U.; Ahlstedt, S. Modification of IgE Binding during Heat Processing of the Cow's Milk Allergen β-Lactoglobulin. *J. Agric. Food Chem.* **2004**, *52*, 1398−1403.
(31) Hamada, D.; Dobson, C. M. A Kinetic Study of beta-Lactoglobulin Amyloid Fibril Formation Promoted by Urea. *Protein Sci.* **2002**, *11*, 2417−2426.
(32) Krebs, M. R. H.; Devlin, G. L.; Donald, A. M. Amyloid Fibril-Like Structure Underlies the Aggregate Structure across the pH Range for beta-Lactoglobulin. *Biophys. J.* **2009**, *96*, 5013−5019.
(33) Lansbury, P. T.; Lashuel, H. A. A Century-Old Debate on Protein Aggregation and Neurodegeneration Enters the Clinic. *Nature* **2006**, *443*, 774−779.
(34) Verheul, M.; Roefs, S.; de Kruif, K. G. Kinetics of Heat-Induced Aggregation of β-Lactoglobulin. *J. Agric. Food Chem.* **1998**, *46*, 896−903.
(35) Le Bon, C.; Nicolai, T.; Durand, D. Growth and Structure of Aggregates of Heat-Denatured β-Lactoglobulin. *Int. J. Food Sci. Technol.* **1999**, *34*, 451−465.
(36) Burgos, I.; Dassie, S. A.; Villarreal, M. A.; Fidelio, G. D. Thermodynamic and Structural Analysis of Homodimeric Proteins: Model of β-Lactoglobulin. *Biochim. Biophys. Acta, Proteins Proteomics* **2012**, *1824*, 383−391.
(37) McKenzie, H. A.; Sawyer, W. H. Effect of pH on β-Lactoglobulins. *Nature* **1967**, *214*, 1101−1104.
(38) Renard, D.; Lefebvre, J.; Griffin, M. C. A.; Griffin, W. G. Effects of pH and Salt Environment on the Association of β-Lactoglobulin Revealed by Intrinsic Fluorescence Studies. *Int. J. Biol. Macromol.* **1998**, *22*, 41−49.
(39) Loupiac, C.; Bonetti, M.; Pin, S.; Calmettes, P. beta-Lactoglobulin under High Pressure Studied by Small-Angle Neutron Scattering. *Biochim. Biophys. Acta, Proteins Proteomics* **2006**, *1764*, 211−216.
(40) Baldini, G.; Beretta, S.; Chirico, G.; Franz, H.; Maccioni, E.; Mariani, P.; Spinozzi, F. Salt-Induced Association of β-Lactoglobulin by Light and X-ray Scattering. *Macromolecules* **1999**, *32*, 6128−6138.
(41) Verheul, M.; Pedersen, J. S.; Roefs, S.; de Kruif, K. G. Association Behavior of Native β-Lactoglobulin. *Biopolymers* **1999**, *49*, 1−20.
(42) Gottschalk, M.; Nilsson, H.; Roos, H.; Halle, B. Protein Self-association in Solution: The Bovine β-Lactoglobulin Dimer and Octamer. *Protein Sci.* **2003**, *12*, 2404−2411.
(43) Townend, R.; Timasheff, S. N. Molecular Interactions in β-Lactoglobulin. 3. Light Scattering Investigation of the Stoichiometry of the Association between pH 3.7 and 5.2. *J. Am. Chem. Soc.* **1960**, *82*, 3168−3174.
(44) Townend, R.; Winterbottom, R. J.; Timasheff, S. N. Molecular Interactions in β-Lactoglobulin. 2. Ultracentrifugal and Electrophoretic Studies of the Association of β-Lactoglobulin Below Its Isoelectric Point. *J. Am. Chem. Soc.* **1960**, *82*, 3161−3168.
(45) Timasheff, S. N.; Townend, R. Structure of β-Lactoglobulin Tetramer. *Nature* **1964**, *203*, 517−519.
(46) Kumosins, T. F.; Timashef, S. N. Molecular Interactions in β-Lactoglobulin. X. Stoichiometry of β-Lactoglobulin Mixed Tetramerization. *J. Am. Chem. Soc.* **1966**, *88*, 5635−5642.
(47) Piazza, R.; Iacopini, S. Transient Clustering in a Protein Solution. *Eur. Phys. J. E* **2002**, *7*, 45−48.
(48) Timasheff, S. N.; Townend, R. The Association Behavior of β-Lactoglobulins-A and β-Lactoglobulins-B. *J. Am. Chem. Soc.* **1958**, *80*, 4433−4434.
(49) Lin, M. Y.; Lindsay, H. M.; Weitz, D. A.; Ball, R. C.; Klein, R.; Meakin, P. Universality of Fractal Aggregates as Probed by Light-Scattering. *Proc. R. Soc. London, Sec. A* **1989**, *423*, 71−87.
(50) Tanford, C.; Kirkwood, J. G. Theory of Protein Titration Curves. 1. General Equations for Impenettrable Spheres. *J. Am. Chem. Soc.* **1957**, *79*, 5333−5339.
(51) Meakin, P. A Historical Introduction to Computer Models for Fractal Aggregates. *J. Sol-Gel Sci. Technol.* **1999**, *15*, 97−117.
(52) Xu, Y.; Mazzawi, M.; Chen, K.; Sun, L.; Dubin, P. L. Protein Purification by Polyelectrolyte Coacervation: Influence of Protein Charge Anisotropy on Selectivity. *Biomacromolecules* **2011**, *12*, 1512−1522.
(53) Navea, S.; Tauler, R.; de Juan, A. Monitoring and Modeling of Protein Processes Using Mass Spectrometry, Circular Dichroism, and Multivariate Curve Resolution Methods. *Anal. Chem.* **2006**, *78*, 4768−4778.
(54) Giger, K.; Vanam, R. P.; Seyrek, E.; Dubin, P. L. Suppression of Insulin Aggregation by Heparin. *Biomacromolecules* **2008**, *9*, 2338−2344.
(55) Kim, A. Y.; Berg, J. C. Fractal Aggregation: Scaling of Fractal Dimension with Stability Ratio. *Langmuir* **2000**, *16*, 2101−2104.
(56) Nozaki, Y.; Bunville, L. G.; Tanford, C. Hydrogen Ion Titration Curves of β-Lactoglobulin. *J. Am. Chem. Soc.* **1959**, *81*, 5523−5529.
(57) Miklavic, S. J.; Chan, D. Y. C.; White, L. R.; Healy, T. W. Double-Layer Forces between Heterogeneous Charged Surfaces. *J. Phys. Chem.* **1994**, *98*, 9022−9032.
(58) Jho, Y. S.; Safran, S. A.; In, M.; Pincus, P. A. Effect of Charge Inhomogeneity and Mobility on Colloid Aggregation. *Langmuir* **2012**, *28*, 8329−8336.
(59) Perkin, S. K., N.; Klein, J. Long-Range Attraction between Charge-Mosaic Surfaces across Water. *Phys. Rev. Lett.* **2006**, *96*, 038301.

(60) Cooper, C. L.; Goulding, A.; Kayitmazer, A. B.; Ulrich, S.; Stoll, S.; Turksen, S.; Yusa, S.; Kumar, A.; Dubin, P. L. Effects of Polyelectrolyte Chain Stiffness, Charge Mobility, and Charge Sequences on Binding to Proteins and Micelles. *Biomacromolecules* **2006**, *7*, 1025−1035.